

Investigation of polylactide and carbon nanocomposite filament for 3D printing

Akshay Potnuru & Yonas Tadesse

Progress in Additive Manufacturing

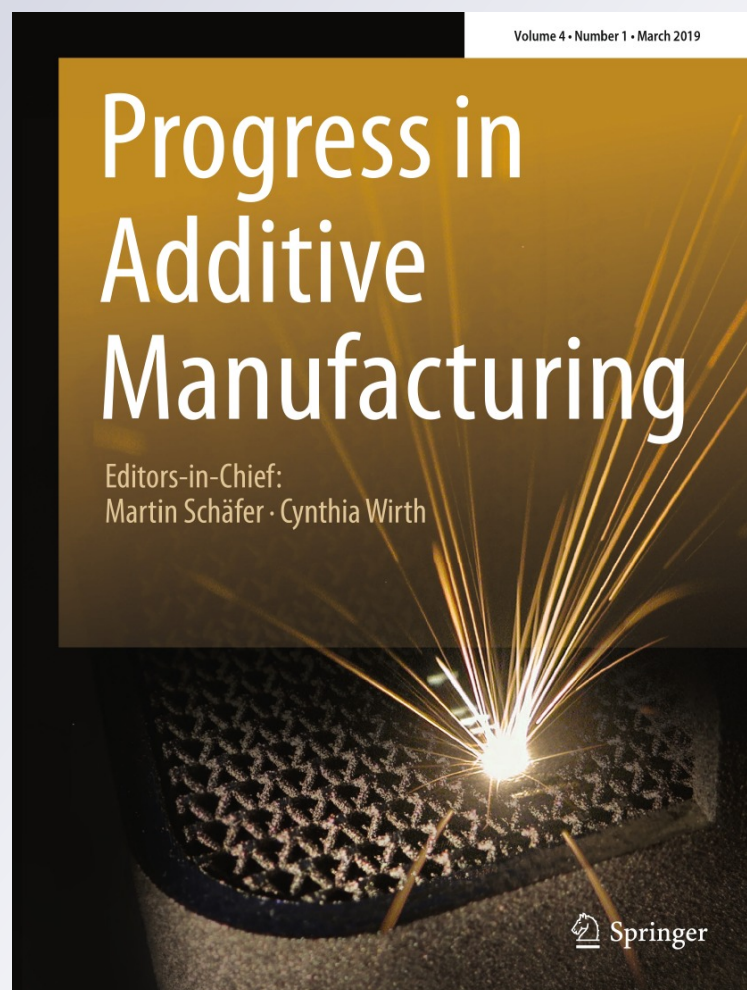
ISSN 2363-9512

Volume 4

Number 1

Prog Addit Manuf (2019) 4:23-41

DOI 10.1007/s40964-018-0057-z



Your article is protected by copyright and all rights are held exclusively by Springer International Publishing AG, part of Springer Nature. This e-offprint is for personal use only and shall not be self-archived in electronic repositories. If you wish to self-archive your article, please use the accepted manuscript version for posting on your own website. You may further deposit the accepted manuscript version in any repository, provided it is only made publicly available 12 months after official publication or later and provided acknowledgement is given to the original source of publication and a link is inserted to the published article on Springer's website. The link must be accompanied by the following text: "The final publication is available at link.springer.com".



Investigation of polylactide and carbon nanocomposite filament for 3D printing

Akshay Potnuru¹ · Yonas Tadesse¹

Received: 23 December 2016 / Accepted: 7 June 2018 / Published online: 19 June 2018
© Springer International Publishing AG, part of Springer Nature 2018

Abstract

Fused deposition modeling (FDM) has been used to manufacture complicated structures and robots in the past few years. However, most FDM machines do not fabricate fully functional robots that are ready for use. One of the requirements of fully functional 3D printed robots is electrical connection in some part of the printed structure. Recently, electrically conductive commercial filaments are emerging to the market, but the actual chemical compositions of the filler and host materials as well as mechanical properties are not available. This paper presents composite materials consisting of conductive carbon nanoparticles, thermoplastics, and solvents to create thin filaments for 3D printing. The mechanical and electrical properties of the filaments fabricated using a composition of 0–15% weight of carbon nanoparticles (NC) in polylactide (PLA) and dichloromethane (DCM) solvent were investigated. The DCM is used for dissolving the PLA and dispersion of the NC, which is subsequently evaporated by drying. The electrical conductivity of the composite filament is compared with commercial and academia counterparts. Possible applications of the composite materials for fabrication of electrical circuitry for 3D printed robots were also discussed.

Keywords Conductivity · 3D printing · Additive manufacturing · Robots · PLA · Carbon nanoparticles

1 Introduction

3D printing is becoming a widely used technology, to develop numerous devices or systems [1], such as robots [2, 3], prosthetics [4, 5], orthosis [6] and skeletal systems [7] using thermoplastic materials mainly. These systems are fabricated using 3D printing and electrical connections are provided by wire systems that result in a shabby and complex system. Hence, there is a need to improve the 3D printing techniques to produce complete models with electronic circuitry for applications such as humanoids. Researchers so far have not found a solution to replace wire with a cheap and effective way. In this work, we present a low-cost alternative

for the problem of robot wiring. Different types of metal 3D printing techniques, which are inherently conductive, exist such as liquid metal printing [8] and direct metal laser sintering [9] for manufacturing strong devices and components. Rosochowski and Matuszak [10] explained many types of rapid prototyping methods among which fused deposition modeling is the most widely used and commercially successful method employed for fabrication of different materials. Inkjet printing technique is another technique used for printing conductive metal patterns for electronic circuitry such as using direct writing of copper. Conductive patterns [11], narrow conductive tracks on untreated polymeric substrates [12] and a complete review of this method are also shown in the past [13, 14]. The major problem in the most commercialized 3D printing techniques for metals (metal 3D printing in particular) is the cost and the high working temperatures, which reduce its portability and affordability.

The different materials that can be 3D printed today are thermoplastics, thermo-polymers, metals, and composite materials. Thermosetting polymers are those that are set irreversibly to solid or semi-solid state in the presence of heat or chemicals such as curing agents generally at ambient temperature [15]. 3D printing is now used for prototyping in

Electronic supplementary material The online version of this article (<https://doi.org/10.1007/s40964-018-0057-z>) contains supplementary material, which is available to authorized users.

✉ Yonas Tadesse
yonas.tadesse@utdallas.edu

¹ Humanoid, Biorobotics and Smart Systems (HBS) Laboratory, Mechanical Engineering Department, The University of Texas at Dallas, 800 W Campbell RD, Richardson, TX 75080, USA

many engineering firms, artist design studios [16], medical tools [17] and for orthopedic implant [18] because of its easy and fast production [1]. Its customizability using direct CAD modeling makes it a major advantage for today's manufacturing process, as even a small change in the product leads to major changes in the production cycle and high financial investments. 3D manufacturing gives the designers flexibility for custom-built structures including complex shapes and multiple material usages which is a major market demand of today and future. Even though significant efforts are made in the 3D printing since its introduction [19], there are several challenges and researches that need to be done to make multifunctional materials.

FDM process uses thermoplastic materials such as acrylonitrile butadiene styrene (ABS), polylactide (PLA), polycaprolactone (PCL) and nylon [33]. The process starts by heating up the thermoplastic to a semi-liquid state ($1\text{ }^{\circ}\text{C}$ higher than the solidification temperature). Then, the 3D printer software uses complex digital modeling data from the CAD file to generate the 3D product layer by layer. Most FDM 3D printers just print the CAD models. Some advanced 3D printers print soluble supporting material in the cavities and supports for complex hanging features of the model to help the model retain its complex shape. The thermoplastic material has a filamentous shape which helps the heat transfer to maintain the semi-liquid state. Filamentous shape assists in the movement of the print head in the x, y and z directions. After printing each layer, a stepper motor connected to screw thread moves the platform down or the head up in z-axis where the distance moved is the thickness of the printed layer. This process is repeated until the entire model is printed. The major benefits of FDM technology are its ease of control, use, maintenance, low cost of the machine and material.

ABS-Cu and ABS-Fe composite filaments were produced by Hwang et al. [20], which were printed by the FDM process to improve thermo-mechanical properties. They showed an improved thermal conductivity and a decrease in mechanical properties of the filament and the printed structure. Carbon fiber-infused ABS filaments were used for 3D printing by Love et al. [21] and they showed an increase in strength, stiffness and thermal conductivity. Mechanical properties of highly filled iron-ABS composites filament were produced by Sa'ude et al. [22] using a mixture of iron powder filled in an ABS and surfactant powder material. A comparison of the effect of incorporating nanoparticles in 3D printing applications was presented by Tsiakatouras et al. [23] consisting of ABS, carbon fiber and carbon nanotubes, and improved mechanical properties were reported. Zhang et al. [24] showed a PLA graphene composite produced by melt extrusion to print complex 3D structures with electrical conductivity. Conductive filaments using 15–20 wt% graphene with polymethyl methacrylate (PMMA) were fabricated by

Nicholson [25]. The resistances were found to be $1.5 \pm 0.4\text{ M}\Omega$ and $60 \pm 7\text{ k}\Omega$ for the 15 and 20 wt% filaments (filament length of 25.4 mm and 1.75 mm in diameter). Graphene and ABS filaments were prepared by Wei et al. [26] similar to the work presented in this paper but using N-Methyl-2-pyrrolidone rather than DCM. Graphene is 5 times expensive than carbon nanoparticles which was used in this paper. A summary of different fillers in thermoplastics and the improved properties are summarized in table. All high-end products these days come with electrical circuitry during manufacturing. FDM uses thermoplastics (insulators), which cannot be used to print the whole functional model with electrical circuitry. The need for making conductive thermoplastic in FDM 3D printing material is the next step to push the 3D manufacturing of complex structures.

Similar work was proposed by the company's Graphene 3D Lab [27], where a commercial plastic/graphene composite filament was used for 3D printing of graphene-enhanced plastic structures. The filament has a volume resistivity of $6 \times 10^{-3}\text{ }\Omega\text{ m}$ and a standard filament diameter of 1.75 mm. The material costs only \$1 per g, but the composition of graphene in the filament is not mentioned. Some of the properties of the filament are not available such as tensile strength. Proto-pasta Conductive PLA is a commercially available conductive filament which is a compound of NatureWorks 4043D PLA and conductive carbon black with a volume resistivity of molded resin (not 3D Printed) of $0.15\text{ }\Omega\text{ m}$ and with a maximum volume resistivity of 3D printed parts through layers (along z-axis) of $1.15\text{ }\Omega\text{ m}$ [34]. Functionalize Electric™ PLA [35], a commercially available conductive filament has a $7.5 \times 10^{-3}\text{ }\Omega\text{ m}$ volume resistivity made from carbon nanotube-based PLA filament. Electrifi filament [36] is another commercially available conductive filament with a resistivity of $6 \times 10^{-5}\text{ }\Omega\text{ m}$ from Multi3d. They have not disclosed their composition of copper and polyester. Sigma-Aldrich has a commercially available carbon nanotube-reinforced polyethylene terephthalate glycol copolymer 3D printing filament trademarked as 3DXNANO™ ESD CNT-PETG, which has a surface resistivity of 10^7 to $10^9\text{ }\Omega$ that was measured using concentric ring test method [37].

Several attempts have been made to produce 3D printable or inkjet printable electrical circuitry. Espalin et al. studied stereo lithography used for 3D printing electronics with the FDM-based system and demonstrated an automated FDM process with the possibility of using direct write for electronic circuitry. In this process, thermoplastics and copper wires were used to increase performance and durability of 3D-printed electronics [38]. Similar work presented in this paper is also shown by Leigh et al. [28]. They demonstrated a concept in 3D printing technology with the formulation of a simple, low-cost conductive composite material (termed 'carbomorph'). They used 15 wt% carbon black in the polycaprolactone (PCL) composite, which falls above

the literature percolation threshold of carbon black in polymer composites [29]. According to [28], higher percentages of carbon black gave a composite that was unable to pass through the standard heated nozzle of a 3D printer and required the nozzle to be drilled out to 1.5 mm diameter and prints to be carried out at 260 °C and above, which significantly compromised print resolution. They presented a 5 mm 3D printed cube that showed an in-plane resistance of $0.09 \pm 0.01 \Omega \text{ m}^{-1}$ and perpendicular to the layers, the resistivity was $0.12 \pm 0.01 \Omega \text{ m}^{-1}$.

This work presents the study of carbon nanoparticles in polylactide (PLA) fiber rather than polycaprolactone (PCL) 3D printable material at various concentrations of carbon nanoparticles. PLA is a more widely used material for 3D printing and has a tensile strength of up to 60 MPa, whereas PCL has a tensile strength of 14 MPa [39]. Furthermore, PLA has shown very good results for the synthesis of polypyrrole (PPy) based composite actuators/artificial muscles [40–42]. The percolation threshold of carbon black in polyethylene is shown by Foulger [43] related to the electrical conductivity of the composites. The percolation threshold is the maximum allowable amount of a filler material inside a host material before the host material starts showing more affinity towards itself and results in a significant drop in resistance depending on the host polymer material.

Morgan et al. presented 3D printed microfluidic devices that were operated using an inexpensive and readily accessible printer [44]. Similar work was also presented by Belter et al. where a technique for increasing the strength of thermoplastic printed parts, by carefully placing voids in the printed parts and filling them with high strength resins was used. They improved the overall part strength and stiffness up to 45 and 25%, respectively [45]. Gao et al. showed high-performance GaIn10-based electrical ink, as both electrical conductors and interconnects. Electrical ink is used for directly writing flexible electronics via a rather simple and cost-effective way, with electrical resistivity measured as $34.5 \times 10^{-8} \Omega \text{ m}$ at 297°K by four-point probe method [46]. Yeo et al. [47] presented a flexible electronics fabrication using direct metal patterning based on laser-induced local melting of the metal nanoparticle ink. Their method was a promising low-temperature alternative to vacuum deposition and photo-lithography based conventional metal patterning processes. They demonstrated high-quality Ag patterning ($2.1 \times 10^{-8} \Omega \text{ m}$) and high-performance flexible organic field effect transistor arrays. Carbon forms in PLA were used in several applications previously. The examples include relative humidity sensor using carbon nanotubes in PLA by Devaux et al. [29]; vapor sensors using PLA multi-wall carbon nanotube (MWCNT) by Kumar et al. [48]; glucose biosensors using PLA/carbon nanotube by Oliveira et al. [30] and more applications are presented by Mukhopadhyay [49]. Hughes et al. [31] fabricated nanocomposite materials using

solvent-cast 3D printing technique of PLA and 5, 10, and 20 wt% MWCNT concentrations. They observed the electrical conductivity at a maximum of 1.21 S/m at 20 wt% MWCNT. The tensile strength increased to 58 MPa for the 5 wt% fiber, while it decreased for the 20 wt% MWCNT. The cost of MWCNT is 5 times more than carbon nanoparticles used in the presented work and, the filaments can be printed in most commercially available FDM 3D printers. Guo et al. [32] made a multifunctional 3D liquid sensor using PLA/MWCNT nanocomposite. They created a helical structure by solvent-cast 3D printing which featured a relatively high electrical conductivity. A comparison literature review is presented in Table 1.

The molecular structure of the presented work substrate materials for filament preparation is shown in Fig. 1, where polylactide $(\text{C}_3\text{H}_4\text{O}_2)_n$ is dissolved in dichloromethane CH_2Cl_2 and mixed with mesoporous carbon nanoparticles. The mesoporous carbon nanoparticles can be described by graphitic structure [50] as shown in Fig. 1. The detailed fabrication will be discussed in the experimental section.

The paper is divided into six sections. Section 1 just highlighted the overall problem, background and the need for the research. Section 2 covers the experimental setup, method and materials. Experimental results such as viscosity, electrical, mechanical and microstructures at different compositions are discussed in Sect. 3. Section 4 has the results and discussion, and Sect. 5 shows the potential application of this study in humanoids and robots to replace wires. Finally, in Sect. 6, the conclusions are provided.

2 Experiments

2.1 Materials

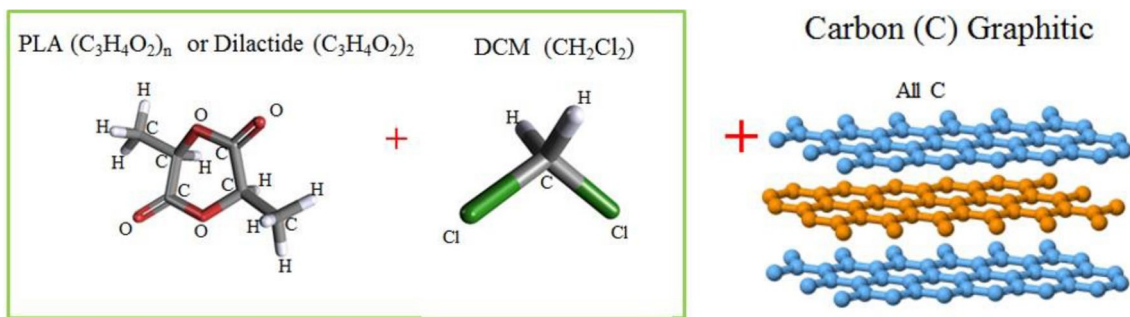
Clear PLA filament of 1.75 mm diameter was purchased from MakerBot Inc.; hot plate with a magnetic stirrer was purchased from VWR International; rubber tubing of 1.75 mm inner diameter was obtained from McMaster-Carr; dichloromethane (DCM), syringes with needles and carbon nanoparticles (carbon, mesoporous nanopowder, graphitized, < 500 nm particle size, > 99.95% trace metals basis) were purchased from Sigma-Aldrich and MakerBot Replicator 2 printer was used for 3D printing.

2.2 Solution preparation for filament

The method is called “Encapsulated Dissolving”, which provides the right viscosity of the PLA/DCM solution for adding mesoporous carbon nanoparticles (NC) later. PLA filaments were cut into small pieces (~ 50 mm on average) and DCM was added in a closed glass container, and then heated. The optimum mixture composition was determined

Table 1 Literature review on additive materials in thermoplastics and the properties improved

Reference	Substrate materials	Additive	Altered property
Hwang et al. [20]	ABS	Cu, Fe	Improved thermal conductivity; decreased in mechanical properties
Love et al. [21]	ABS	Carbon fiber	Increase in strength, stiffness, thermal conductivity
Sa'ude et al. [22]	ABS	Fe powder + surfactant powder	Improved in mechanical properties
Tsiakatouras et al. [23]	ABS	Carbon fiber + carbon nanotubes	Improved in mechanical properties
Zhang et al. [24]	PLA	Graphene	Improved in electrical properties
Nicholson [25]	Polymethyl methacrylate (PMMA)	15–20 wt% graphene	Improved in electrical properties
Wei et al. [26]	ABS	Graphene + N-methyl-2-pyrrolidone	Improved in electrical properties
Graphene 3D Lab [27]	PLA	Graphene	Improved in electrical properties
Leigh et al. [28]	Polycaprolactone (PCL)	15 wt% carbon black	Improved in electrical properties
Devaux et al. [29]	PLA	Carbon nanotubes	For relative humidity sensor
Oliveira et al. [30]	PLA	Carbon nanotubes	For glucose biosensors
Hughes et al. [31]	PLA	MWCNT	Improved in electrical properties; improved in mechanical properties
Guo et al. [32]	PLA	MWCNT	Improved in electrical properties; multifunctional 3D liquid sensor

**Fig. 1** The molecular structures of the materials used for filament preparation. The major process includes dissolving biodegradable thermoplastic polylactide (PLA) with dichloromethane (DCM) and adding mesoporous carbon nanoparticles (NC)

to be 1:5 weight ratio of PLA and DCM for the experiments till 6 wt% of NC and PLA. This ratio gave a good viscosity for casting in a rubber mold and making functional filament. The ratio was determined by trial and error, using a particular composition and checking if solid filament or partially solid filaments can be obtained in 24 h drying time. The heating of the solution with closed lid adds DCM vapors in the chamber, which was used to dissolve the long un-submerged PLA inside the glass. The nanoparticles were added after the PLA was fully dissolved, which took about half the time of the synthesis. The solution is left alone for 5 min for the DCM vapors to settle down. The synthesis time is also proportional to the amount of PLA used, which means smaller samples take less time. Table 2 shows the PLA and carbon nanoparticles' proportions, and the relative time of preparation. The time of preparation is relative to the ratio of PLA and DCM. There are several major advantages of this method: no wastage of DCM due to evaporation in

Table 2 The composition of materials studied, which include various carbon nanoparticles (NC) proportions in 1 gram of PLA

Percentage by weight (NC:PLA)%	Carbon nanoparticles (g)	Dichloromethane (mL)	Relative time of preparation (min)
0	0	5	20
0.5	0.005	5	20
1.5	0.015	5	20
6 ^a	0.06	5	20
9	0.09	7.5 ^b	17
15	0.15	10 ^b	15

^aThe 6 wt% filaments were not 3D printable for testing

^bThe DCM volume was increased to keep the viscosity in the optimum value for solid filaments.

the process of solution preparation; no need to pre-cut small pieces of PLA to submerge and dissolve; and the controlled amount of the contents in the solution. The PLA pieces can be cut as big as the base of the glass. The un-submerged PLA is dissolved by the DCM vapors trapped inside. Large amounts of PLA and NC solutions can be prepared for large filament samples. Other advantages include simpler procedure, repeatable with no need of constant observation to estimate the right viscosity range. In Table 2, we have presented only the compositions which yielded to a 3D printable filament. At 3% weight ratio we can get the viscosity of the composition, but it did not yield in a functional filament. Hence, the 3% weight ratio falls in low viscosity region, which has only a 50% probability of success. Targeting the medium viscosity (1600–2200 mPa s) has the best yield for final filaments, which will be discussed in Sect. 3.1. The

prepared solution can be stored with closed lid for next usage before drying (2 days to 2 weeks depending upon the sealing of the container). Video of the entire process is provided as Supplementary File: S1 Video.

2.3 Filament preparation

Figure 2 shows the experimental procedure of solution preparation, injection of the solution into a rubber tube, and 3D printing. First, the PLA/NC/DCM solution was mixed with the magnetic stirrer as described in the previous section. Next, the solution was taken from the glass using syringes and injected into a 1.75 mm rubber tube from both sides for uniform distribution of pressure. Holes were punched in the middle of the tube for the DCM to evaporate. Finally, the setup was left for 24 h. for drying in a fume hood. The

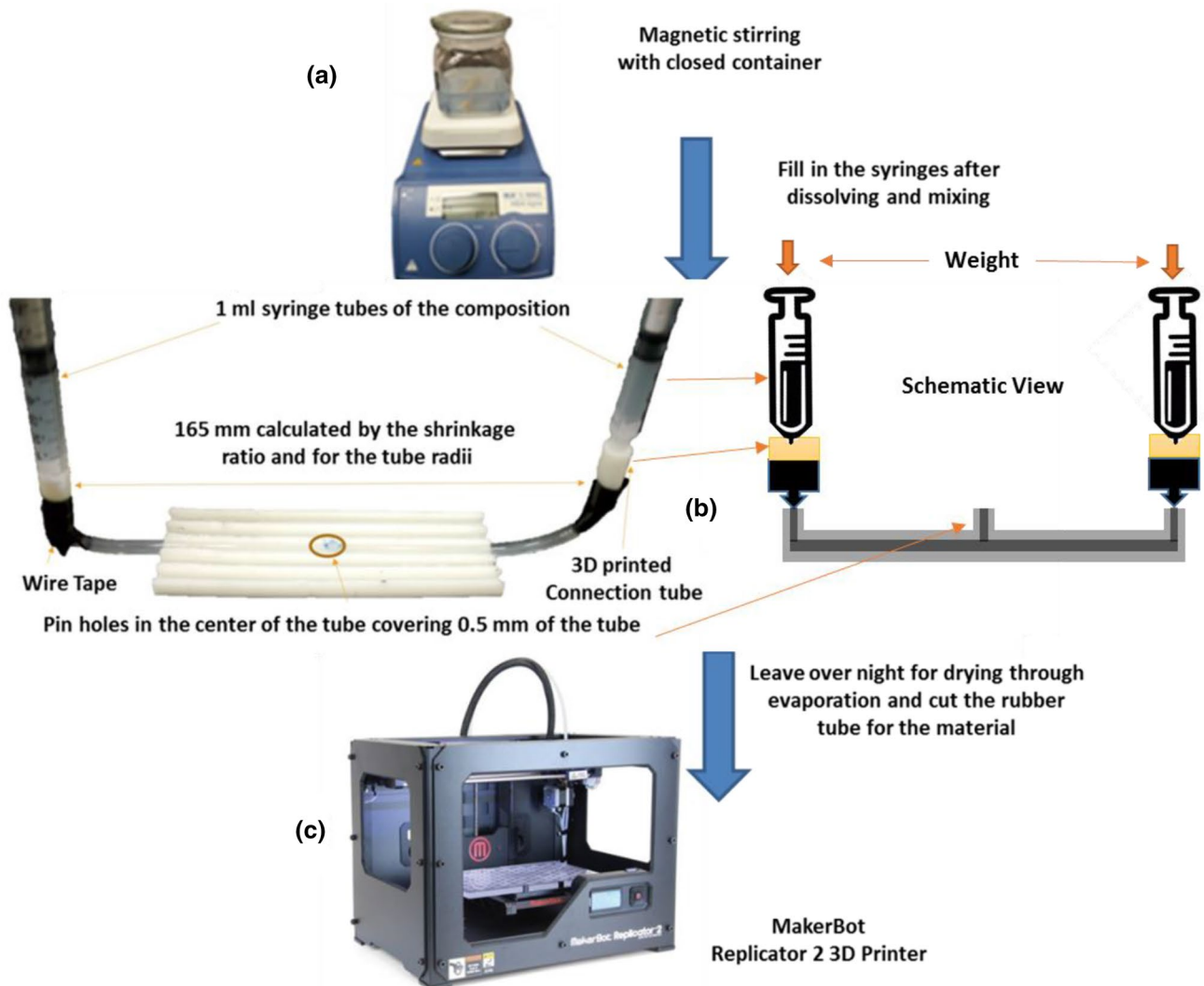


Fig. 2 Preparation of composite filaments and 3D printing. **a** Magnetic stirring with closed container, **b** picture of the drying technique and schematic view and **c** MakerBot Replicator 2 3D printer used for printing the filaments

filament was taken out of the mold (This will be discussed later). Similar solution blending technique was used when grafting a PLA to carbon nanoparticle surfaces for bio-nanocomposites preparation [51]. PLA is a biodegradable and bio-compatible material that can be used for diverse applications.

Several experiments were conducted to observe the volume shrinkage of the solution prepared during the evaporation (horizontal drying) process of the DCM. The volume shrinkage was observed to be 1:5 PLA and DCM volume ratio. This ratio helps in understanding how much dried filament sample can be made from a given solution mixture. The syringe is connected to the 1.75 mm rubber tube using a 3D printed connector of varying holes on both ends for uniform distribution and tightly sealed using wire tape. To get 165 mm long solid filament, two syringes were used with 1 mL solution in each syringe and then injected into the rubber tube from both sides as shown in Fig. 2. The major advantages of horizontal drying are that the nanoparticles will be properly distributed throughout the tube rather than vertical drying, where the nanoparticles

coagulate at the bottom due to gravity. This effect is prominent as the drying time is around 24 h. Pressure on both ends eliminated the air bubbles while open-ended tubes without pinholes showed tunneling effect. Tunneling effect is the process of evaporation of the solution inside the tube creating a tunnel in the filament. This results in hollow filaments that are unsuitable for printing. The tube is kept inside a 3D printed frame structure for proper holding of the tube in shape. The pin holes (~ 0.5 mm diameter) are kept only at the center of the tube on the open side rather than all over the tube, which gave sufficient outlet for the DCM to evaporate.

Figure 3 shows the designed 3D printed load carrier structures for proper compression of the rubber tube throughout the drying process. The calibrated weights are used as a load and are applied from the top at both ends. A hole is inbuilt in the design for vertical assembly of the structure on the stand to the required calibrated weight dimensions. A hole is also provided to hold the syringes in position while drying. These stands are custom designed for different weights and syringes. The loads were varied from 0.75 to 1.25 kg as

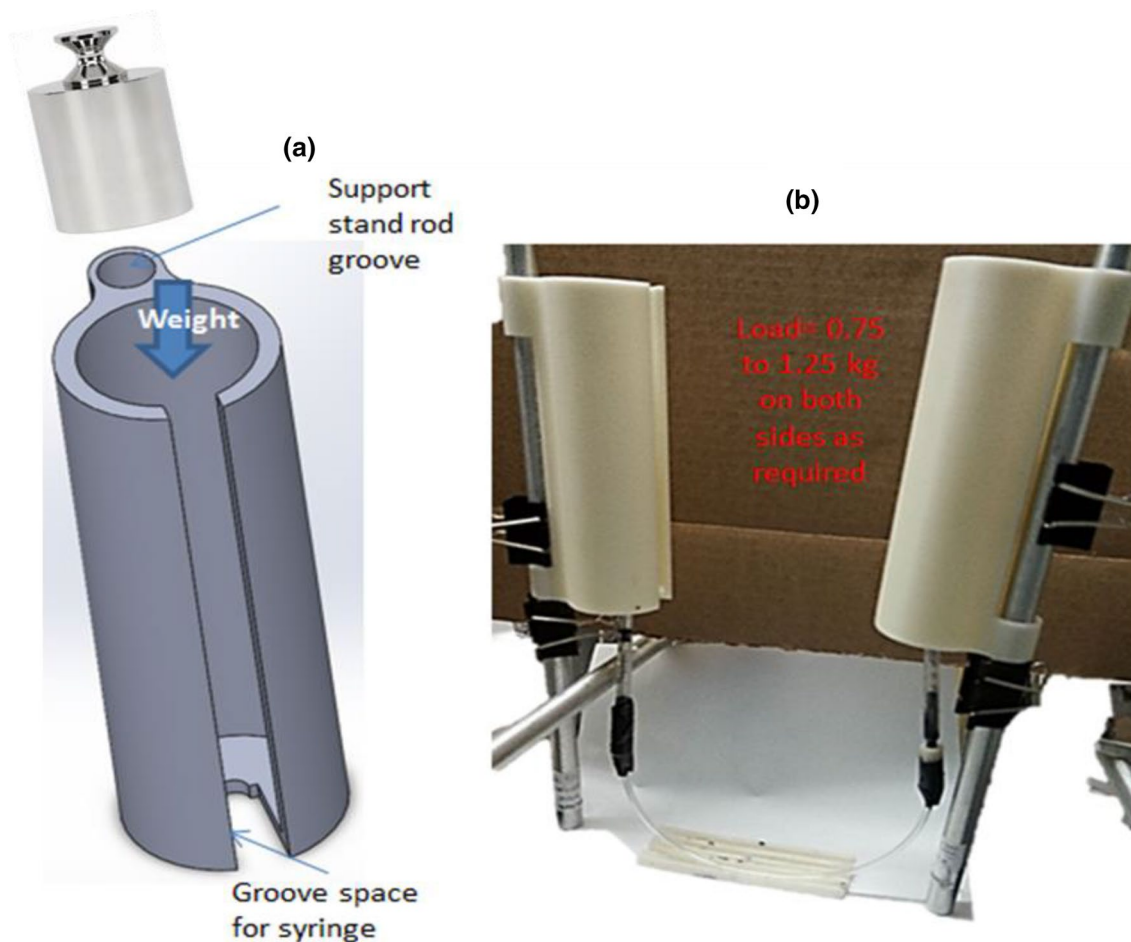


Fig. 3 a 3D printed load carrier structures, b full horizontal drying setup with weights

required for different compositions. The drying time with NC was around 24 h and without NC it was around 12 h.

The cutting technique uses a 3D printed blade casing which cuts the rubber tube to its thickness on both sides with high precision. Figure 4 shows the SolidWorks 2014 CAD design of the cutting apparatus. This can be modified for different rubber tubes as required. This design is made for 1.75 mm inner diameter rubber tubes obtained from McMaster. The apparatus is assembled using screws and bolts with Dewalt carbide utility blade. The design is made in such a way that the blade is firmly held in the groove exposing sufficient tip to cut. The tube is pre-cut for about 20 mm before pushing through the hole for proper alignment of the blade tips to cut the tube. The protruded part of the tube can be used to firmly hold and pull the tube out. The tube is pulled out by an impulse movement with sufficient force, which cuts the tube and leaves the filament untouched. The blades can be replaced when blunt and the technique needs minimum hand skills of the user, making the process extremely fast and simple.

2.4 Long filament fabrication

The longer filament (1.5 m in length) was made through implementation of spring-loaded mechanism with same holders as shown in Fig. 3a. The spring load mechanism is shown in Fig. 5a, where cuts were made using a Dremel at three different points, each representing the zero loads for 7, 4, and 0 mL solution. The spring load system was adapted for longer filaments, as calibrated weight loads required for long filaments were too heavy. The spring was held between spring holders and rubber bands to give more strength to withhold the tension caused by the spring on

the 3D printed holder. The springs used were 22.2 mm in diameter and 101.6 mm in size applied on both ends with a safe working load limit of 24.8–44.7 lbs. (11.8–20 kg). The holder was designed to hold 60 mL standard syringes. In the case of the longer filaments, in the middle along the length of 30 mm, a cluster of pinholes were punched as it required more DCM to evaporate. Figure 5b shows the complete setup of the injection and drying mechanism. Figure 5c illustrates the synthesized 1.5 m long filament for big size 3D prints. It took 4 days for drying compared to 1–2 days of drying for the smaller filaments. This can be controlled by the pin holes or by implementing forced drying techniques. The forced drying techniques can also change the strength and properties of the formed filament. The fume hood used had a maximum exhaust flow of 645.5 CFM and average face velocity of 131.5 FPM. The current technique in this paper illustrates the method of improving the properties of thermoplastic materials with nanomaterials as additives or fillers. The process can be scaled up for mass manufacturing by employing a good drying technique, because the current longtime requirement for longer filament is due to the need of cooling techniques. Another issue was the 3D printed connectors, which were made of ABS, eroded during drying due to DCM exposure for long hours and needed to be replaced several times to avoid leakages. This can be resolved using porcelain connectors, as it does not react with DCM.

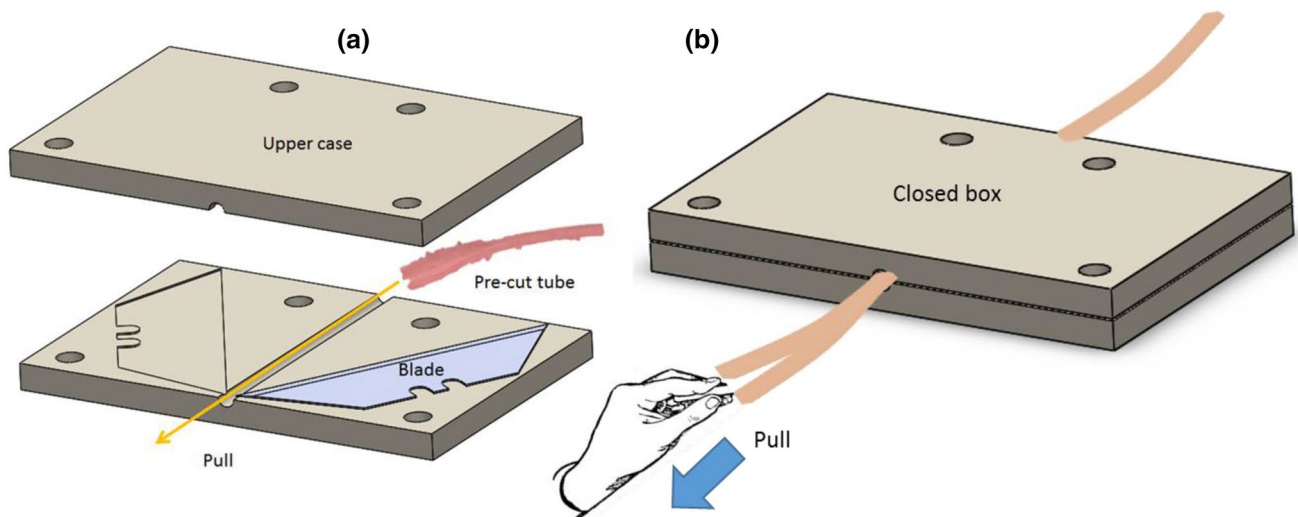


Fig. 4 **a** SolidWorks 2014 CAD model of the cutting apparatus for splicing the rubber mold that has initial pre-cut. **b** Assembled cutting apparatus when the rubber tube is pulled by hand

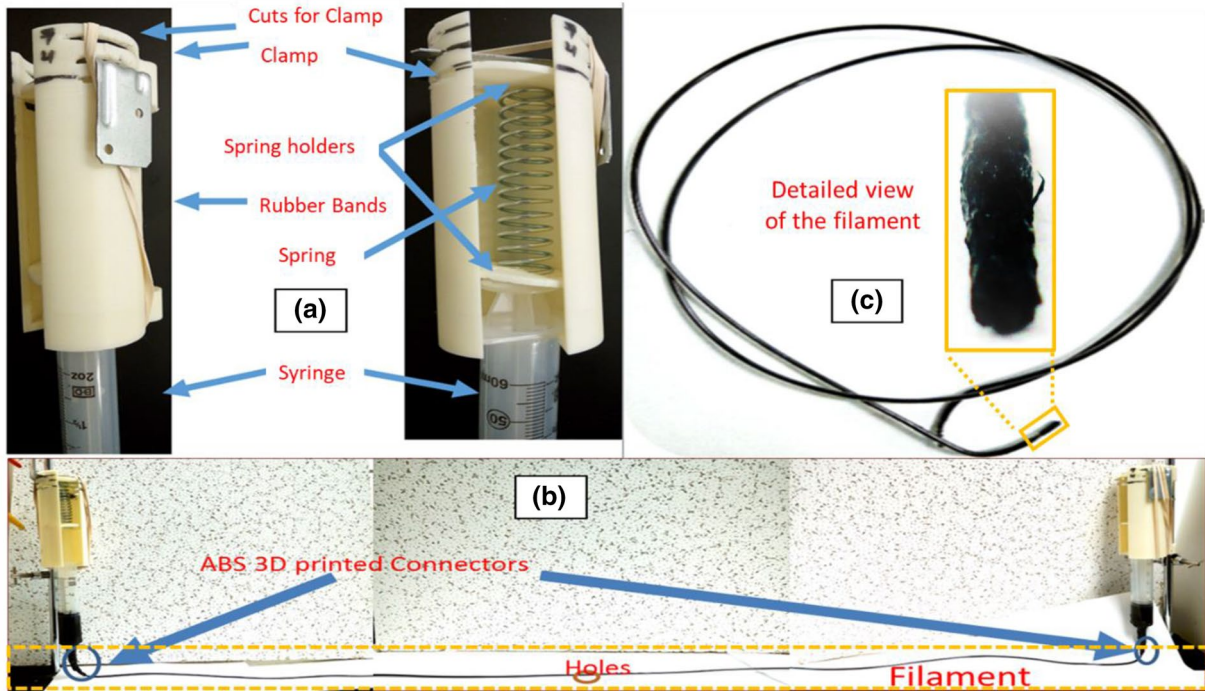


Fig. 5 a The spring mechanism implemented in the holders for more load, b a 1.5 m long filament preparation using spring mechanism and c the prepared long filament

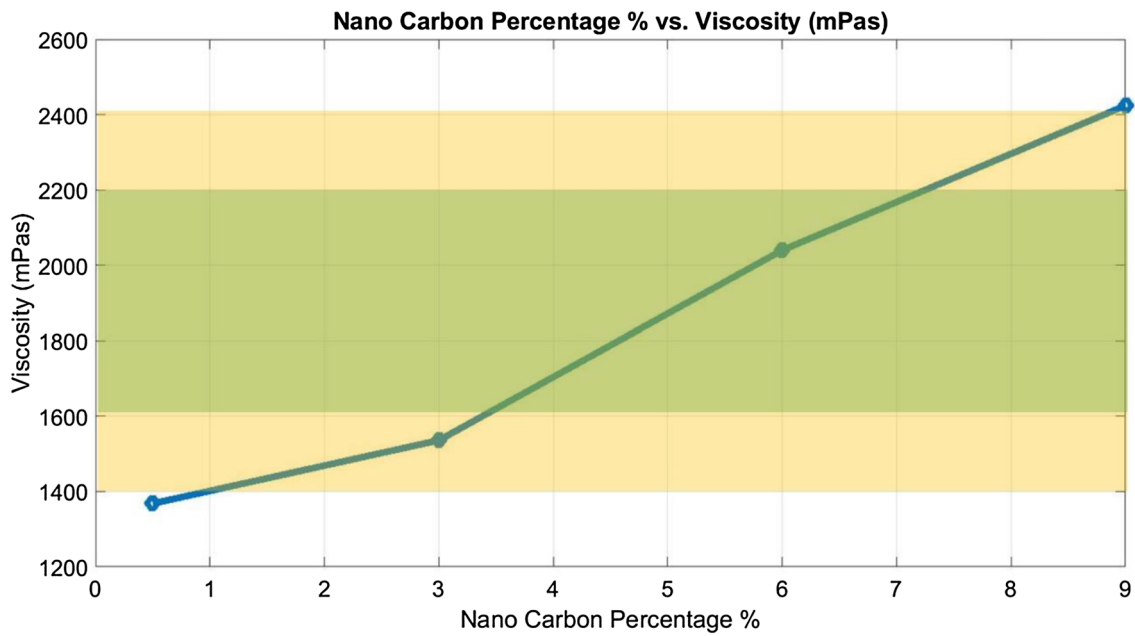


Fig. 6 Viscosity (mPa s) of carbon nanoparticles percentage for 1 g PLA and respective volumes of DCM from Table 2 at 25 rpm and at room temperature for 1:5 weight ratio

3 Experimental results

3.1 Viscosity of PLA, NC and DCM solution

Figure 6 shows the typical viscosity range of 0–15 wt% of carbon nanoparticles in PLA in 5–10 mL DCM solution as shown in Table 2. These data were obtained from Brookfield DV2T viscometer. The typical viscosity, that can be used for solution casting, is between 1400 and 2400 mPa s (or cP) shown in a transparent green box and the optimum range for proper filament samples was 1600–2200 mPa s shown in a transparent orange box. Beyond this, the solution is out of viscosity range for preparation of solid filament which is visually and experimentally observed. This phenomenon is controlled by increasing the DCM volume as shown earlier in Table 2. The 9 and 15 NC wt% have a higher amount of DCM to control the viscosity in the favorable range. The variation implies that the viscosity increases as the percentage of nano-carbon increases, which matches with general observation as the volume of nanoparticles increases as percentage increases [52]. All the experiments were done under a chemical hood. If the optimum viscosity range is crossed, it will be too dry to suck through a syringe. If the solution is too viscous, after evaporation in the rubber tubing, it will reduce in volume leaving air cavities and eventually giving a hollow, brittle and weak filament which is unusable with the 3D printer.

3.2 Electrical property of the PLA and carbon nanoparticles composite filaments

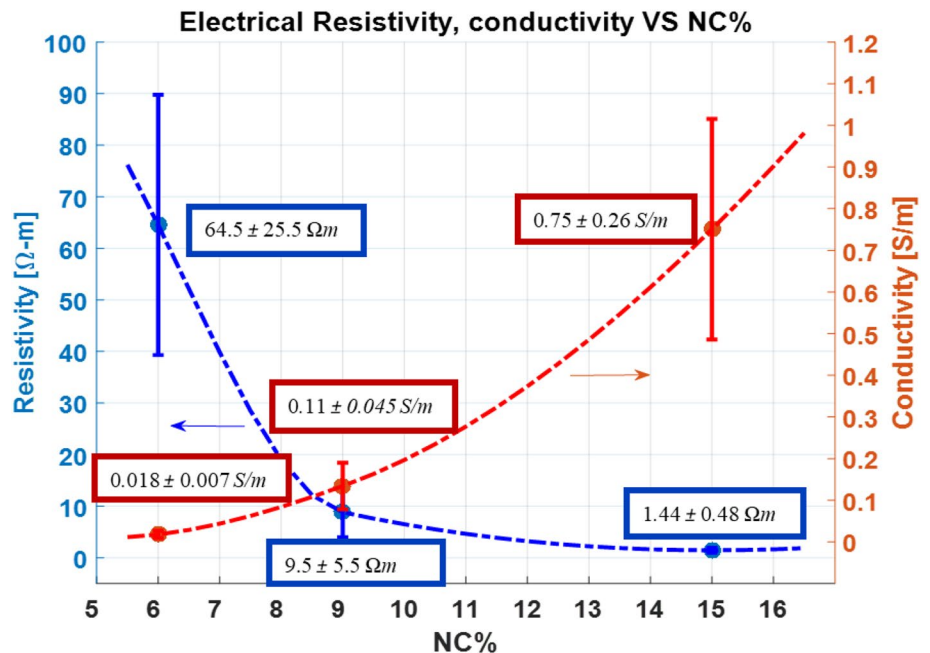
Electrical conductivity tests of the composite filaments consisting of PLA and carbon nanoparticles were done using radio shack voltmeter to find the resistance at 10 mm apart across the length of the sample and the average values were taken. The measurements were taken several times and on different dates as well. The average values and the standard deviations of both the resistivity and conductivity results are shown in Fig. 7. As expected, the conductivity of the filaments increases as the percentage of the carbon nanoparticles increases.

The relationship of geometrical properties and material constant can be expressed by the following simple equation:

$$k = \frac{1}{\rho} = \frac{1}{RA}, \tag{1}$$

where k is the conductivity, ρ is the resistivity, R is the resistance, L is the length, and A is the area of the sample. In Fig. 7, the average electrical resistance of a filament with a diameter of 1.75 mm and measured at 10 mm distance along the longer filament made from at 15 wt% NC was 6 ± 2 k Ω . This resistance is equivalent to a resistivity of 1.44 ± 0.48 Ω m and conductivity of 0.75 ± 0.26 S/m, which is significantly lower from infinite resistance as PLA is a pure insulator. In Fig. 7, the comparison is done under the same conditions for different percentages of the NC. The inconsistencies are due to non-uniform formations of the filament because of human error. The major error is due to measurement of the electrical resistivity which was done at different

Fig. 7 Resistivity and conductivity of the filaments made of various wt% of carbon nanoparticles in PLA. The samples were 1.75 mm in diameter and 100 mm long, where the resistances of each sample were taken at 10 mm distance along the filament, both the average and standard deviation of the measurement are shown



segments in a long filament and taking the average and standard deviation. Since the distribution of the conductive part was not uniform for a different composition, the large deviation is prevalent in Fig. 7. The electrical conductivity at a low weight percentage of the filler carbon nanoparticles was observed at 6 wt%, which is low compared to the works presented by others.

The resistances shown by Nicholson [25] with graphene and PMMA composite were $1.5 \pm 0.4 \text{ M}\Omega$ and $60 \pm 7 \text{ k}\Omega$ for the 15 and 20 wt% filaments of length 25.4 mm and diameter of 1.75 mm, which is equivalent to $142 \text{ }\Omega \text{ m}$ or $7 \times 10^{-3} \text{ S/m}$ for 15 wt% sample and $5.7 \text{ }\Omega \text{ m}$ or 0.18 S/m for 20 wt% sample. The resistance of their sample at 15 wt% is very high compared to the presented results. Zhang et al. [24] at 6 wt% graphene and PLA filament showed conductivity of 13 S/m , whereas our sample conductivity is $0.02 \pm 0.01 \text{ S/m}$ for 6 wt% NC and PLA. In a similar study, Wei et al. [26] showed electrical conductivity of $1.05 \times 10^{-3} \text{ S/m}$ at 5.6 wt% graphene and ABS composite, which is low compared to the presented work. The conductivity of molded resin (not 3D printed) of Proto-pasta Conductive PLA is 6.67 S/m [34] which is better than

the presented work, but the weight percentage of carbon black used is not specified. Functionalize Electric™ PLA [35], a commercially available conductive filament has a 133.3 S/m which is better than the presented work, but as mentioned previously carbon nanotubes are expensive than carbon nanoparticles and the composition is also not specified. 3DXNANO™ ESD CNT-PETG [37] has a high surface resistivity of 10^7 to $10^9 \text{ }\Omega$ (tested using concentric ring test method) which is comparatively higher, but this is not compared as the volume resistivity is not specified. Graphene 3D Lab [27], a commercial plastic/graphene composite filament used for 3D printing of graphene-enhanced plastic structures has a conductivity of 166.7 S/m which is better than the resistivity presented in this paper, but the composition and all properties are not disclosed. Similarly, Electrifi filament [36] is another commercially available conductive filament made with biodegradable polyester and copper with a conductivity of $16,667 \text{ S/m}$, but they do not disclose its composition. In Fig. 8, a comparison of the conductivity of nano-additives in host thermoplastic polymer compared with the work presented in this paper is shown. This figure is a

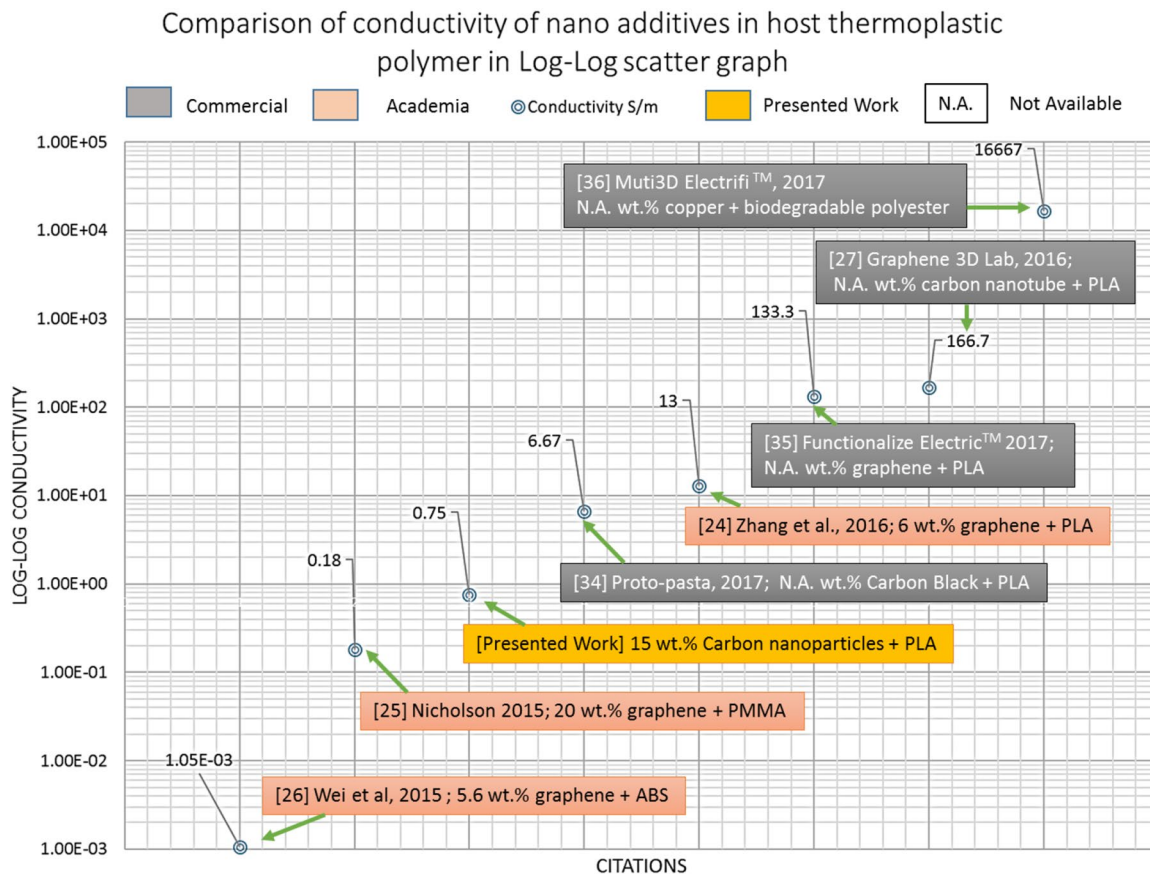


Fig. 8 Comparison of the conductivity of nano-additives in host thermoplastic polymer [24–27, 34–36]. The commercially available filaments are shown in grey, the academically published filaments are shown in salmon color and the presented work is shown in mustard color

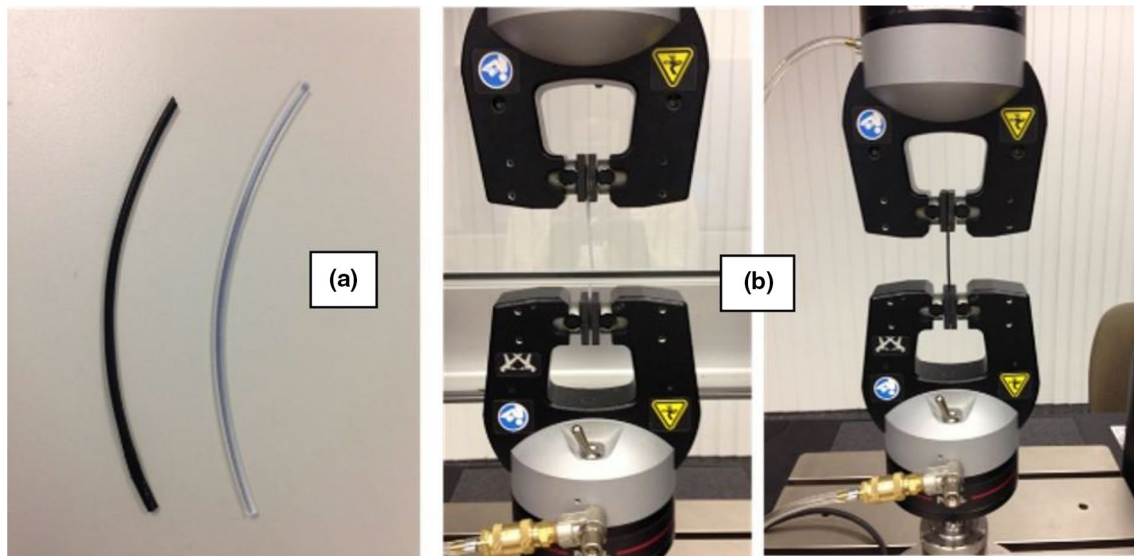


Fig. 9 Tensile testing of **a** Clear PLA (right) and 15 wt% NC and PLA (left) samples, **b** clear PLA (left) and 15 wt% NC and PLA (right) testing

summary of the discussion in this section, which will provide insightful information to readers.

3.3 Mechanical property of the PLA and carbon nanoparticles composite filaments

To study the mechanical strength of the filaments, Instron tensile tester (5960 dual column) was used to test their ultimate tensile strength and compared with original PLA (commercially obtained) and PLA samples prepared with DCM at various NC compositions (0, 0.5, 1.5, 9 and 15 wt% NC: PLA). In Fig. 9, tensile testing of (a) clear PLA (right) and 15 wt% NC and PLA (left) samples are shown and in (b) clear PLA (left) and 15 wt% NC and PLA (right) test setups are shown, respectively. In Fig. 10, the tensile strength of NC1.5 is higher than that of NC0.5 which could be reinforcement provided by carbon at some small values and the role of DCM with plastic with NC filler needs to be further studied. The tensile test was quasi-static at a strain rate of 1 mm/min. In Fig. 10a, the stress–strain curves of all the samples along with a 3D printed dog bone structure (NC15 3D, printed with 15 wt% NC filament) is shown. The inset of stress–strain is also shown for all except PLA and 3D printed part. The pure PLA has the highest strength of 60 MPa, and most of the samples have below 15 MPa strength. However, the 3D printed structure using 15 wt% NC: PLA filament has the 25 MPa tensile stress. Using the presented manufacturing process from Fig. 10b, the reader can see a small drop in the mechanical strength as more carbon nanoparticles are added in PLA. The 3D printed part is stronger due to the dog bone structure printed in layers. Table 3 shows the values of ultimate tensile stress and strain, respectively, for

each sample. There is a significant loss of tensile strength when DCM is used for dissolving the PLA and adding the NC using the presented manufacturing process. Effect of strength using other solvents can be studied in future using this method. The 6 wt% filament was not tested because at this diameter the filament was non-uniform. Three samples from each composition were fabricated, but the tensile tests were done using the best samples from each (one sample) as most of them broke before reaching the maximum tensile load during testing (Fig. 10).

3.4 Microstructure of filaments

Scanning electron microscope (SEM) images of the samples were taken and shown in Fig. 11a. In Fig. 11a, the dark structures are mostly insulating PLA and the bright structures are the conductive carbon. In Fig. 11b, the reader can observe a bar graph of particle distribution of nanoparticles in the respective SEM images that were processed in MATLAB image processing toolbox [53], where the number of the particles increases as the percentage of carbon nanoparticles in PLA increases. A similar representation of SEM imaging in particle distribution histogram was shown in another study of thermoplastic nanocomposites with carbon nanotubes [54]. A clear increase of the white formations is observed, as the percentage of the carbon nanoparticles increases in the sample. One more observation is that the carbon nanoparticles are seen coagulated and the surface has platelet formation with the increase of carbon nanoparticles.

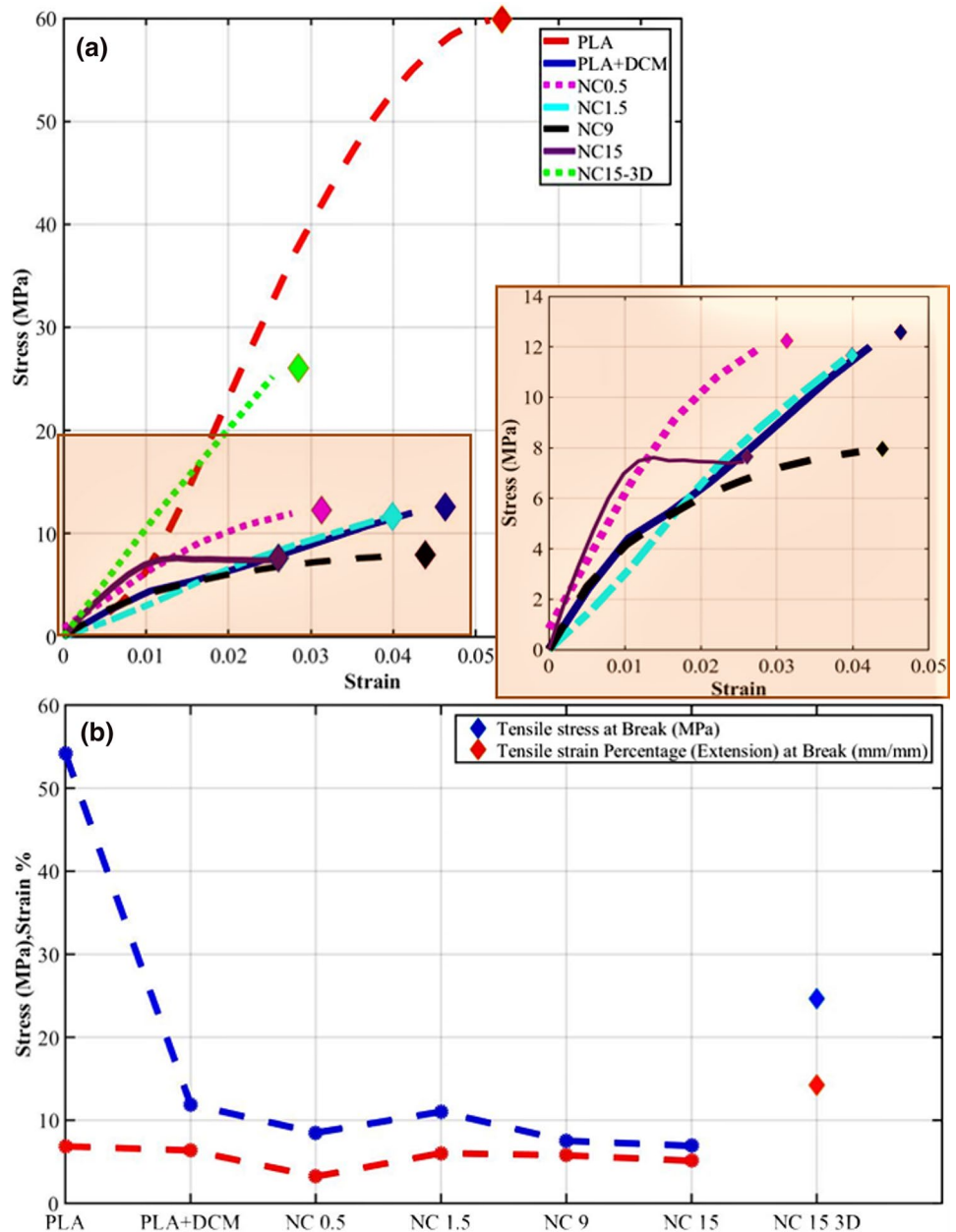
Low-resolution images of samples at lower NC concentration is observed. Figure 12a shows the streaked surface of clear PLA made through commercial hot extrusion and

Table 3 Tensile test results of all the PLA/DCM/NC specimens of 1.75 mm diameter

S. no.	Specimen label	Tensile stress (ultimate) [MPa]	Ultimate tensile strain [mm/mm]
1	Pure PLA	54.2	0.069
2	NC0	11.9	0.064
3	NC0.5	8.5	0.032
4	NC1.5	11.0	0.060
5	NC9	7.5	0.058
6	NC15	6.9	0.051

Fig. 12c shows the 15 wt% NC (NC15) at a lower resolution (bar scale = 100 μm) where one can clearly see the NC coagulated structures. Due to horizontal drying, the reader can also see more NC concentration towards the right of the picture representing the bottom of the tube due to the weight of NC and vice versa, and more PLA towards the left or top of the tube can be observed. The reader should not be confused with a bright glare as NC, as it just represents the reflection of the electron beam in the SEM machine. SEM images of PLA and Arlcel 83 in a solvent of dichloromethane (DCM) and toluene were shown by Liu et al. [55], where PLA micro-capsules

Fig. 10 Mechanical property of filaments made of various compositions of wt% NC in PLA **a** tensile stress–strain curve (diamond marker shows tensile stress (MPa) and tensile strain (%) at the break for all samples with along with a 3D printed structure



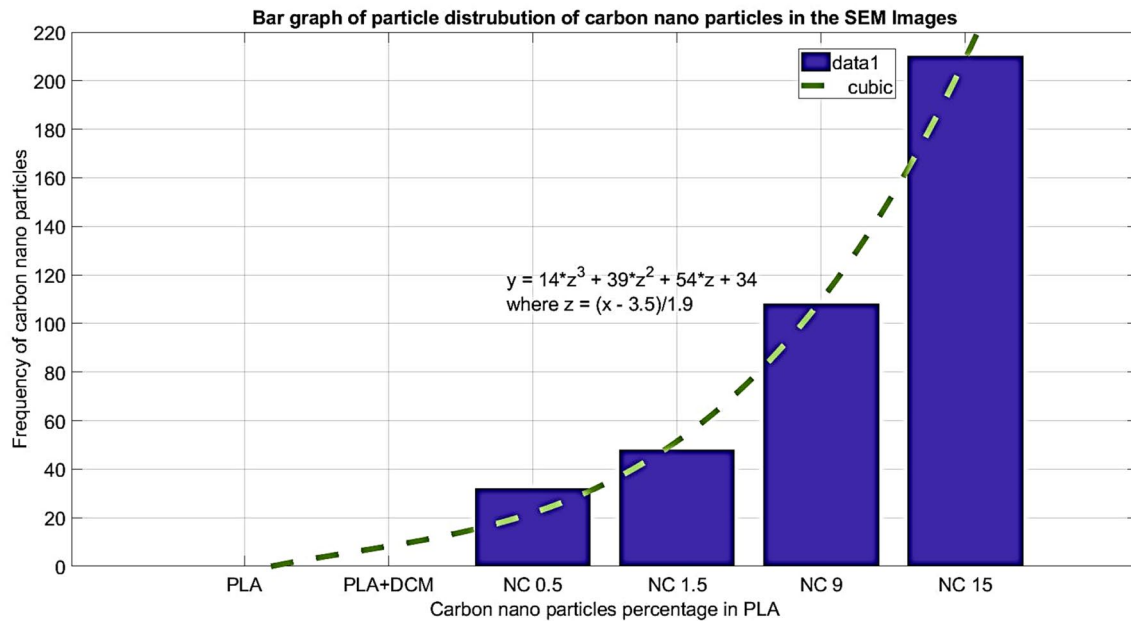
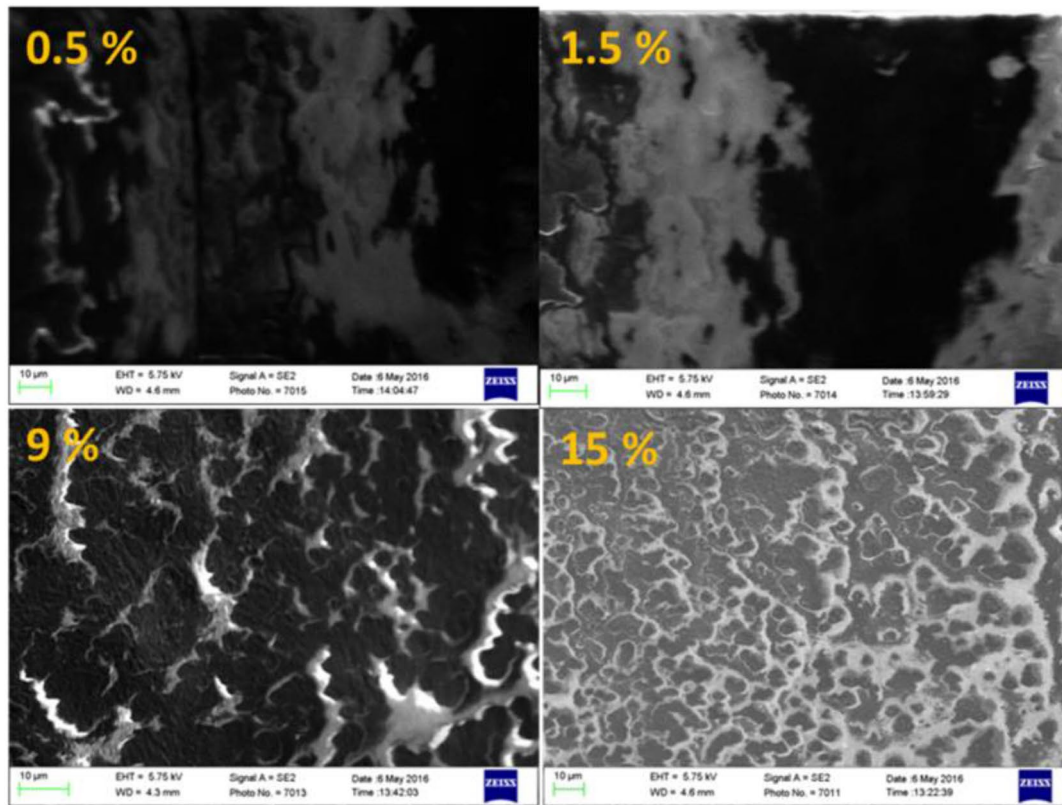
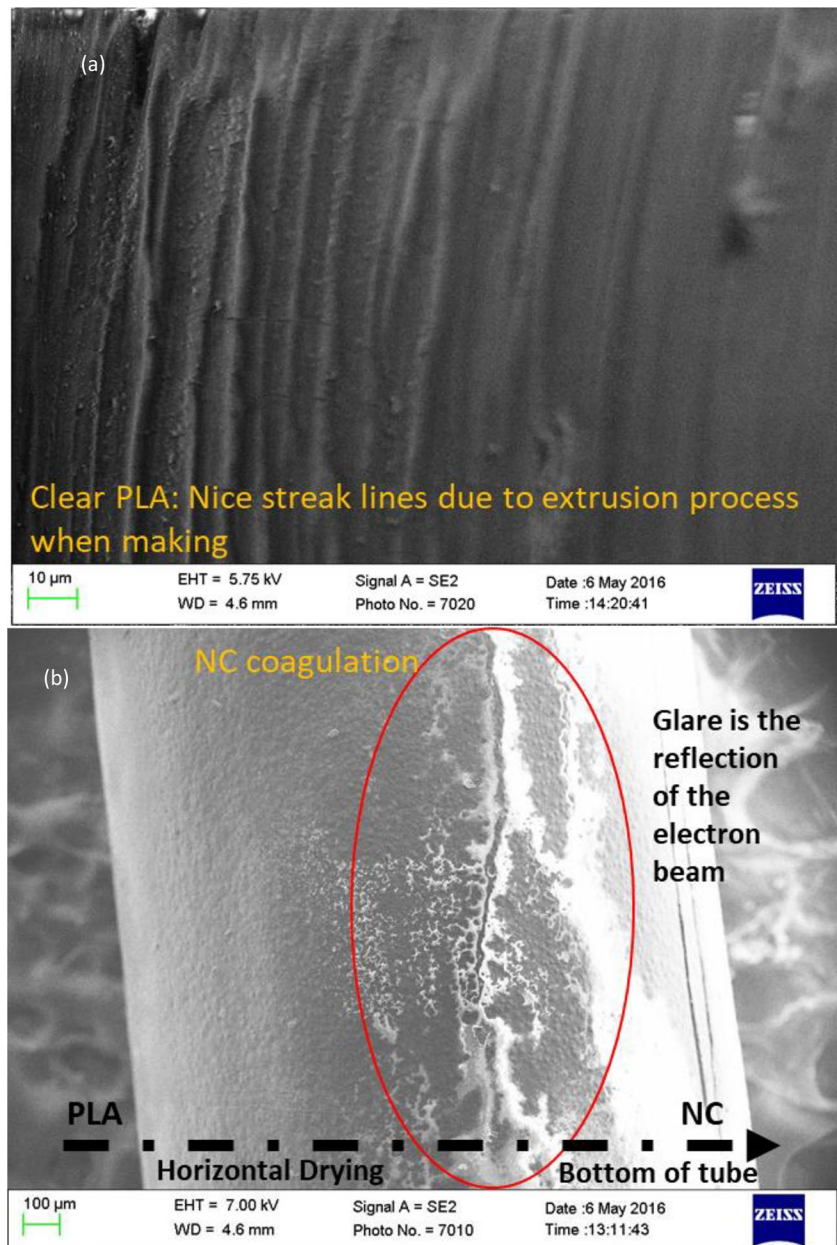


Fig. 11 Microscopy and image analysis of various wt% of NC in PLA along the surface: (left) SEM images of the filaments of NC0.5, NC1.5, NC9 and NC15 at 10 μm resolution; and (right) bar graph of particle distribution of nanoparticles in the respective SEM images

formation and variable distribution exist due to the solvents and compositions. Similar SEM image as in Fig. 11 is also presented by Haroosh et al. [56], where they showed for PLA: PCL blends in DCM: DFM except

few fibrous structures due to electro-spinning and solution contents. Utilizing inkjet 3D printing, Jakus et al., also showed related SEM images of samples made of PLG–graphene using DCM [57]. The variation in texture

Fig. 12 SEM images of samples at the surface: **a** clear PLA and **b** SEM image of NC15 at lower resolution showing the effects of horizontal drying



in the presented work samples is because of the horizontal drying process in a tube that resulted in a smooth surface.

In Fig. 13, one can see the SEM images of the cross-section of the filament from NC0.5, NC1.5, NC9 and NC15 compositions at 100 μm resolution. The plasticity of NC0.5 and NC1.5 that bent the filaments while slicing them for SEM images can be observed in Fig. 13. The brittleness of NC9 and NC15 due to increased carbon helps in a cleaner cut. The SEM images are sharper as the NC percentage or conductivity of the filament increases.

4 Observations and discussions

Several methods and approaches were investigated to successfully synthesize a solid filament with various percentages of carbon nanoparticles using a DCM solvent. The most successful method is described earlier in the section. Then, the filaments are characterized for strength and electrical conductivity. As shown in Fig. 7 earlier, low percentage of NC (6 wt%) showed large standard deviation

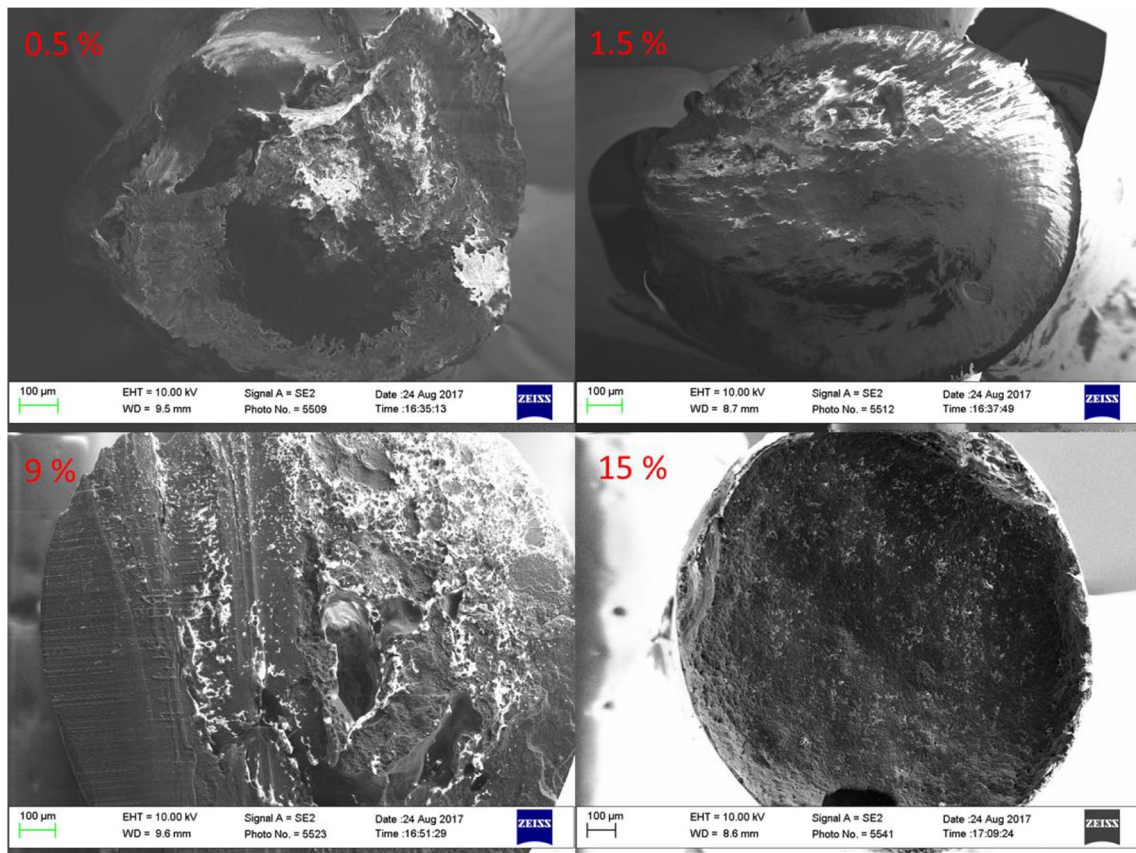


Fig. 13 Microscopy and image analysis of various wt% of NC in PLA: (left) SEM images of the filaments of NC0.5, NC1.5, NC9 and NC15 at 100 μm resolution in cross-sectional view

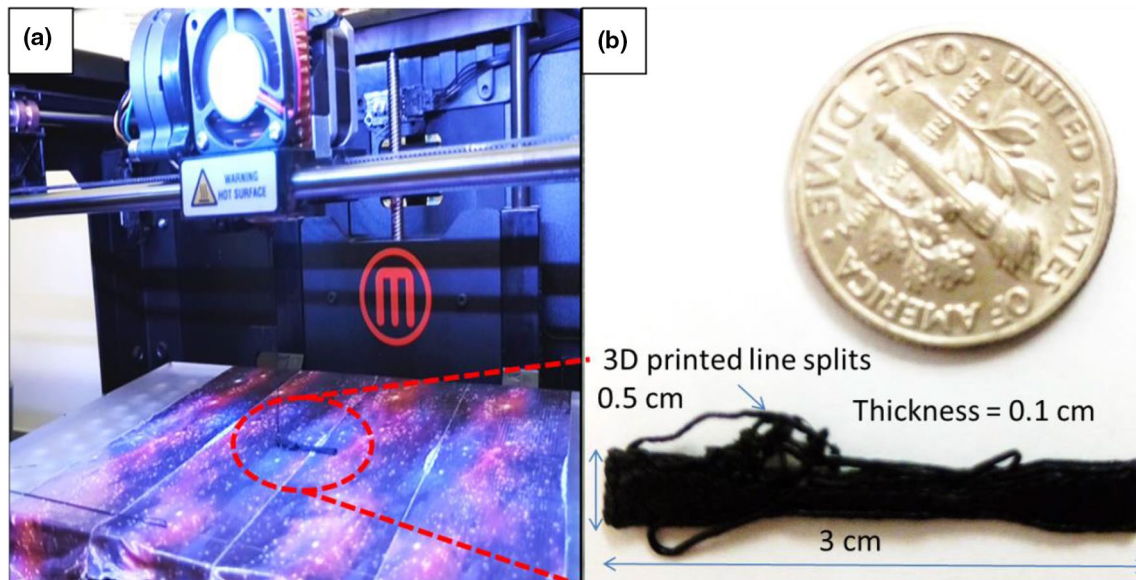


Fig. 14 **a** MakerBot 3D printer test system and **b** 30 mm×5 mm×1 mm dog bone structure printed from a composition of 15 wt% carbon nanoparticles and polylactide fiber (PLA) using MakerBot 3D printer

in resistivity due to the variation of carbon distribution across the surface. However, the variation decreases with a higher concentration of NC. Among the samples, the 15 wt% NC filament was used to 3D print a dog bone structure for demonstration. Initially, several attempts with different filaments that have either void inside or not completely solid brought difficulty in 3D printing using commercial 3D printers. The main issue was that the extrusion force between two gears damaged the filaments and created difficulty in extruding out the new filaments. Therefore, care was taken for fabrication of solid filaments. The 15 wt% NC mixed in PLA solution was selected for 3D printing due to the relatively high conductivity of the filament as discussed previously.

The video of the printing is provided in the Supplementary File: S2 Video. The 15 wt% NC PLA filaments had an average resistivity of $1.44 \pm 0.48 \Omega \text{ m}$ or conductivity of $0.75 \pm 0.26 \text{ S/m}$, whereas clear PLA had infinite resistance. Figure 14 shows the 3D printed dog bone structure of 30 mm in length, 5 mm in width and 1 mm in thickness (the measured resistance was $118 \pm 64 \text{ k}\Omega$). The deduced resistivity and conductance of the dog bone structure was slightly higher ($20 \pm 10 \Omega \text{ m}$ and $0.065 \pm 0.04 \text{ S/m}$), as there was a rearrangement of carbon nanoparticles while 3D printing. This is lower than 476 S/m at 6 wt% of reduced graphene oxide (r-GO) in PLA after 3D printing is shown by Zhang et al. [24], but their filament conductivity was 13 S/m , whereas the presented work is $0.75 \pm 0.26 \text{ S/m}$ with the same 3D printer in both cases, but different chemicals and parameters were used during synthesis. The cost of PLA filament per g is roughly 0.6 cents from MakerBot Inc. and the cost of mesoporous carbon from Sigma-Aldrich is roughly \$30 per g. Hence, the NC15 material cost would be roughly \$5 per g. Assuming for cost analysis that they purchased from same sources in 2018, reduced graphene oxide (r-GO) used by Zhang et al. [24] from Sigma-Aldrich roughly costs \$750 per g. Hence, NC15 costs 9 times lesser than the 6 wt% of reduced graphene oxide (r-GO) in PLA of Zhang et al. [24]. The authors synthesized their own reduced graphene oxide, but the cost analysis was done to get a good comparison based on the available material in the market. While 3D printing the sample, the filament was melted in the 3D printer head without a proper distribution of carbon nanoparticles (uncontrolled) and resulted in a higher electrical resistance. On the other hand, Wei et al. [26] at 3.8 wt% graphene in ABS composite showed a conductivity of $6.4 \times 10^{-5} \text{ S/m}$ and after it was 3D printed into 10 mm x 10 mm x 1 mm rectangular model, the conductivity decreased to $2.5 \times 10^{-7} \text{ S/m}$. Again assuming similar cost analysis, graphene and ABS cost roughly \$1200 per g from Sigma-Aldrich and 0.5 cents per g from MakerBot Inc., which brings their filament per g roughly 9 times more expensive than NC15 presented in this paper. This shows that the 3D printing process must

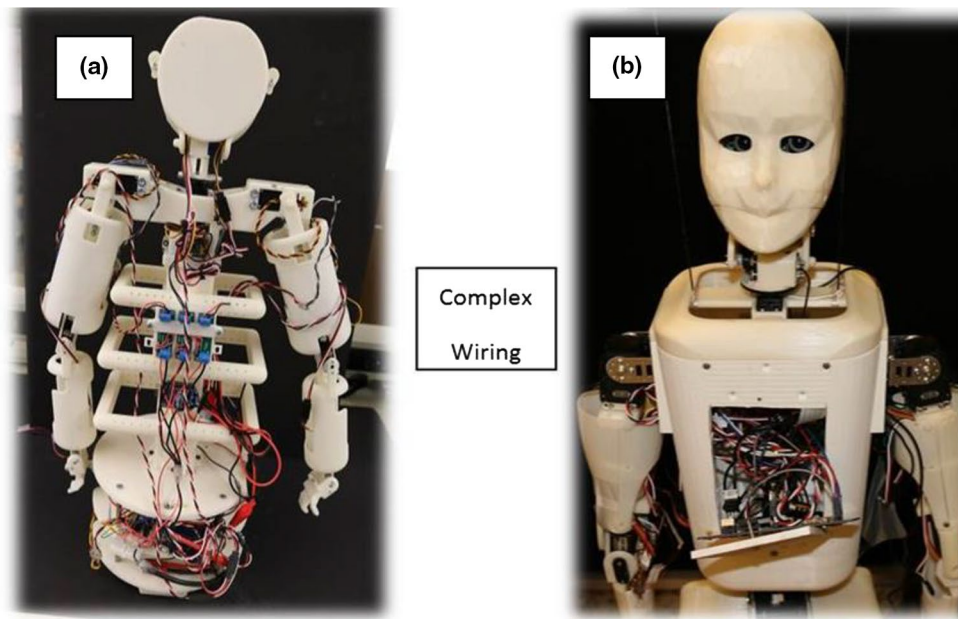
be optimized for homogeneous melting for better conductive 3D printed parts. As mentioned before, the mechanical strength of the filaments is reduced as the amount of the carbon nanoparticles is increased, which has become a challenge when 3D printing using MakerBot 3D printer. The problem was that the filament having more than 15 wt% carbon nanoparticles was not strong enough to pass through the extruder head. This was also observed by Zhang et al. [24] and they could not go beyond 8 wt% in their case. The major difference is that they used hot melt extrusion using HAAKE twin-screw melt mixer, while in this work DCM solution blending is used. Solution blending may give more freedom of higher concentrations of the filler and more uniform distribution. As mentioned previously, carbon nanoparticles are 5 times cheaper than graphene, making the procedure presented in this paper more cost-efficient.

The approach in this paper could be a cheap alternative to regularly used gold-coated electrodes. This method provides an advantage such as the ability to get 3D printable complex shape electrodes. The only limitation of this method is the clogging of the 3D printer head due to successive printing with coated NC and PLA filament which leaves a residue that is very adhesive in nature and becomes very hard after drying. To unclog the nozzle, DCM was used and the nozzle can be used again after several hours of soaking. A nano-lubricant inside the nozzle would solve this issue of clogging. The first layer of the printed structure (Fig. 14b) did not stick to the base of the 3D printer, which left a dangling structure. This can be easily resolved using adhesive tapes available in the market for the 3D printers.

5 Application in humanoids

One application of the conductive filament is in the fabrication of robots and humanoids. Humanoids are robots, which look and perform like humans. They are often made of several mechanical and electrical parts having complex electrical wires running from the power sources, controllers and actuators. As the humanoids are expected to perform complex tasks using complex manner like humans, these complex network wires cause a major problem as they become dangled near the joints and along the whole body. In our experience, these wires end up tangled and detach during complex human-like movements causing failure and repeatable maintenance and low productivity. The work presented in this paper has high application in humanoids that use 3D printing as its major manufacturing technology. This can be implemented in the humanoids like Buddy [3, 58, 59] and HBS-1 [2] humanoid, which are mostly 3D printed using ABS plastic for various applications. As shown in Fig. 15, wires can be replaced by printing conductive filaments to complete the electrical circuits of components, which do not

Fig. 15 Complex wiring examples of 3D printed humanoid **a** front side of Buddy-3D printed humanoid having mobile base [58], **b** a child-size humanoid, HBS-1 similar in size to a 7-year old, 3D printed in the HBS laboratory [2]



interfere or be a hindrance during the complex maneuver of the robot. Wires can also run through the pipe segments to minimize tangling at the joints. NC printed wiring can solve the major problem of actuation, maintenance and connection issues, ultimately leading to advancement in humanoid manufacturing. This can be implemented on any 3D printed parts to avoid wiring and utilize the advantages of the concept. Due to higher resistance than regular copper wires, there can be a decrease in power efficiency which is a limitation. This can be solved by conducting more research in the fillers rather than carbon nanoparticles like gold, silver nanoparticles, etc., which have higher electrical conductivity, but this will increase the overall cost.

6 Conclusions

A composite material consisting of carbon nanoparticle (NC), dichloromethane (DCM) and polylactide (PLA) was made for use as filament material for application in additive manufacturing and the material was characterized extensively. The electrical conductivity and mechanical properties of the filament material were experimentally measured for various weight percentages of mesoporous carbon nanoparticles in polylactide matrix. It was found that the synthesized filaments had a mechanical strength of 12 MPa than the original solid PLA filament (60 MPa), but the electrical resistivity was improved from infinite to a range of 64 ± 25 to $1.4 \pm 0.48 \Omega \text{ m}$ for 6–15 wt% NC: PLA composition. A sample structure of $30 \times 5 \times 1 \text{ mm}^3$ was 3D printed and tested for mechanical strength and resistivity and found to be 25 MPa and $20 \pm 10 \Omega \text{ m}$, respectively. SEM images showed

a relatively large number of particles distributed across the filament for a higher concentration of NC. The method can be used to build the robot structures with electrical circuitry except at the joints. The connection at joints can be made by a jumper that maintains continuous contact as discussed in the paper. This approach reduces the problem of dangling and detachment of wires often encountered in many robotic systems. This work is easy to implement with any 3D printed structures that need electronic circuitry in an economical way using commonly used 3D printers. Future of this project is the implementation of the technique presented in robotics and other complex wiring applications.

Acknowledgements Part of this work is supported by the Office of Naval Research (ONR), Young Investigator Program, under the Grant Number N00014-15-1-2503.

References

1. Bak D (2003) Rapid prototyping or rapid production? 3D printing processes move the industry towards the latter. *Assemb Autom* 23(4):340–345
2. Wu L, Larkin M, Potnuru A, Tadesse Y (2016) HBS-1: a modular child-size 3D printed humanoid. *Robotics* 5(1):1
3. Potnuru A, Jafarzadeh M, Tadesse Y (2016) 3D printed dancing humanoid robot “Buddy” for homecare. In: 2016 IEEE international conference on automation science and engineering (CASE). IEEE, pp 733–738
4. Arjun A, Saharan L, Tadesse Y (2016) Design of a 3D printed hand prosthesis actuated by nylon 6–6 polymer based artificial muscles. In: 2016 IEEE international conference on automation science and engineering (CASE). IEEE, pp 910–915
5. Saharan L, Tadesse Y (2016) Robotic hand with locking mechanism using TCP muscles for applications in prosthetic hand and

- humanoids. SPIE smart structures and materials + nondestructive evaluation and health monitoring, 2016. International Society for Optics and Photonics, 97970V–97979
6. Saharan L, Sharma A, de Andrade MJ, Baughman RH, Tadesse Y (2017) Design of a 3D printed lightweight orthotic device based on twisted and coiled polymer muscle: iGrab hand orthosis. SPIE smart structures and materials + nondestructive evaluation and health monitoring. International Society for Optics and Photonics, pp 1016428–1016410
 7. Tadesse Y, Wu L, Saharan LK (2016) Musculoskeletal system for bio-inspired robotic systems. *Mech Eng* 138(3):S11
 8. Ladd C, So JH, Muth J, Dickey MD (2013) 3D printing of free standing liquid metal microstructures. *Adv Mater* 25(36):5081–5085
 9. Khaing M, Fuh J, Lu L (2001) Direct metal laser sintering for rapid tooling: processing and characterisation of EOS parts. *J Mater Process Technol* 113(1):269–272
 10. Rosochowski A, Matuszak A (2000) Rapid tooling: the state of the art. *J Mater Process Technol* 106(1):191–198
 11. Park BK, Kim D, Jeong S, Moon J, Kim JS (2007) Direct writing of copper conductive patterns by ink-jet printing. *Thin Solid Films* 515(19):7706–7711
 12. Van Osch TH, Perelaer J, de Laat AW, Schubert US (2008) Inkjet printing of narrow conductive tracks on untreated polymeric substrates. *Adv Mater* 20(2):343–345
 13. Kamyshny A, Steinke J, Magdassi S (2011) Metal-based inkjet inks for printed electronics. *Open Appl Phys J* 4:19–36
 14. Bikas H, Stavropoulos P, Chryssoulouris G (2016) Additive manufacturing methods and modelling approaches: a critical review. *Int J Adv Manuf Technol* 83(1–4):389–405
 15. Irfan M (2012) Chemistry and technology of thermosetting polymers in construction applications. Springer, Dordrecht
 16. Walters P, Huson D, Parraman C, Stanić M (2009) 3D printing in colour: technical evaluation and creative applications. In: Impact 6 international printmaking conference
 17. Rengier F, Mehndiratta A, von Tengg-Kobligk H, Zechmann CM, Unterhinninghofen R, Kauczor H-U, Giesel FL (2010) 3D printing based on imaging data: review of medical applications. *Int J Comput Assist Radiol Surg* 5(4):335–341
 18. Krzyzanowski M, Svyetlichnyy D, Stevenson G, Rainforth WM (2016) Powder bed generation in integrated modelling of additive layer manufacturing of orthopaedic implants. *Int J Adv Manuf Technol* 87:519–530
 19. Horvath J (2014) A brief history of 3D printing Mastering 3D printing. Springer, Berlin, pp 3–10
 20. Hwang S, Reyes EI, Moon K-S, Rumpf RC, Kim NS (2015) Thermo-mechanical characterization of metal/polymer composite filaments and printing parameter study for fused deposition modeling in the 3D printing process. *J Electron Mater* 44(3):771–777
 21. Love LJ, Kunc V, Rios O, Duty CE, Elliott AM, Post BK, Smith RJ, Blue CA (2014) The importance of carbon fiber to polymer additive manufacturing. *J Mater Res* 29(17):1893–1898
 22. Sa'ude N, Ibrahim M, Ibrahim MHI (2013) Mechanical properties of highly filled iron-ABS composites in injection molding for FDM wire filament. In: Materials Science Forum, 2013. Trans Tech Publications, Zurich, pp 448–453
 23. Tsiakatouras G, Tsellou E, Stergiou C (2014) Comparative study on nanotubes reinforced with carbon filaments for the 3D printing of mechanical parts. *Trans Eng Technol Edu* 12(3):392–396
 24. Zhang D, Chi B, Li B, Gao Z, Du Y, Guo J, Wei J (2016) Fabrication of highly conductive graphene flexible circuits by 3D printing. *Synth Met* 217:79–86
 25. Nicholson JC (2015) Nanoenhanced additive manufacturing: additive introduction onto halloysite nanotubes and into 3D printing filament for tailored material characteristics. Louisiana Tech University, Ruston
 26. Wei X, Li D, Jiang W, Gu Z, Wang X, Zhang Z, Sun Z (2015) 3D printable graphene composite. *Sci Rep* 5:1118
 27. Graphene 3D Lab Inc. (2016) Conductive graphene filament. <http://www.graphene3dlab.com/s/filament.asp>. Accessed 30 Sept 2016
 28. Leigh SJ, Bradley RJ, Purssell CP, Billson DR, Hutchins DA (2012) A simple, low-cost conductive composite material for 3D printing of electronic sensors. *PLoS ONE* 7(11):e49365
 29. Devaux E, Aubry C, Campagne C, Rochery M (2011) PLA/carbon nanotubes multifilament yarns for relative humidity textile sensor. *J Eng Fiber Fabr* 6:13–15
 30. Oliveira JE, Mattoso LHC, Medeiros ES, Zucolotto V (2012) Poly(lactic acid)/carbon nanotube fibers as novel platforms for glucose biosensors. *Biosensors* 2(1):70–82
 31. Vincent-Hughes IT, Kambiz C, Daniel T (2016) 3D printable conductive nanocomposites of PLA and multi-walled carbon nanotubes. *Mater Matters* 11:2
 32. Guo S-z, Yang X, Heuzy M-C, Therriault D (2015) 3D printing of a multifunctional nanocomposite helical liquid sensor. *Nanoscale* 7(15):6451–6456
 33. Novakova-Marcincinova L, Kuric I (2012) Basic and advanced materials for fused deposition modeling rapid prototyping technology. *Manuf Ind Eng* 11(1):24–27
 34. Proto-pasta Conductive PLA. <https://www.proto-pasta.com/pages/conductive-pla>. Accessed 20 Aug 2017
 35. Functionalize-Electric™ PLA. <http://functionalize.com/about/functionalize-f-electric-highly-conductive-filament/>. Accessed 8 Aug 2017
 36. Multi3D. <https://www.multi3dllc.com/product/electrifi-3d-printing-filament/>. Accessed 20 Aug 2017
 37. 3DXNANO™ ESD CNT-PETG carbon nanotube reinforced polyethylene terephthalate glycol copolymer 3D printing filament. http://www.sigmaaldrich.com/catalog/product/aldrich/3dxcn003?lang=en®ion=US&cm_sp=Insite_-_recent_fixed_-_recent5-2. Accessed 23 Aug 2017
 38. Espalin D, Muse DW, MacDonald E, Wicker RB (2014) 3D printing multifunctionality: structures with electronics. *Int J Adv Manuf Technol* 72(5–8):963–978
 39. Averous L, Moro L, Dole P, Fringant C (2000) Properties of thermoplastic blends: starch–polycaprolactone. *Polymer* 41(11):4157–4167
 40. Potnuru A, Tadesse Y (2014) Synthesis and characterization of hybrid actuator based on polypyrrole and SMA. ASME 2014 international mechanical engineering congress and exposition, 2014. American Society of Mechanical Engineers, p V003T003A003
 41. Tadesse Y, Brennan J, Smith C, Long TE, Priya S (2010) Synthesis and characterization of polypyrrole composite actuator for jellyfish unmanned undersea vehicle. In: Proceedings of SPIE, the international Society for Optical Engineering, 2010. Society of Photo-Optical Instrumentation Engineers, Bellingham
 42. Tadesse Y, Grange RW, Priya S (2009) Synthesis and cyclic force characterization of helical polypyrrole actuators for artificial facial muscles. *Smart Mater Struct* 18(8):085008
 43. Foulger SH (1999) Electrical properties of composites in the vicinity of the percolation threshold. *J Appl Polym Sci* 72(12):1573–1582
 44. Morgan AJ, San Jose LH, Jamieson WD, Wymant JM, Song B, Stephens P, Barrow DA, Castell OK (2016) Simple and versatile 3D printed microfluidics using fused filament fabrication. *PLoS ONE* 11(4):e0152023
 45. Belter JT, Dollar AM (2015) Strengthening of 3D printed fused deposition manufactured parts using the fill compositing technique. *PLoS ONE* 10(4):e0122915

46. Gao Y, Li H, Liu J (2012) Direct writing of flexible electronics through room temperature liquid metal ink. *PLoS ONE* 7(9):e45485
47. Yeo J, Hong S, Lee D, Hotz N, Lee M-T, Grigoropoulos CP, Ko SH (2012) Next generation non-vacuum, maskless, low temperature nanoparticle ink laser digital direct metal patterning for a large area flexible electronics. *PLoS ONE* 7(8):e42315
48. Kumar B, Castro M, Feller J-F (2012) Poly(lactic acid)-multi-wall carbon nanotube conductive biopolymer nanocomposite vapour sensors. *Sens Actuators B* 161(1):621–628
49. Mukhopadhyay S (2011) *Nanoscale multifunctional materials: science & applications*. Wiley, New York
50. Liang C, Li Z, Dai S (2008) Mesoporous carbon materials: synthesis and modification. *Angew Chem Int Ed* 47(20):3696–3717
51. Sobkowicz MJ, Dorgan JR, Gneshin KW, Herring AM, McKinnon JT (2009) Supramolecular bioNanocomposites: grafting of biobased polylactide to carbon nanoparticle surfaces. *Aust J Chem* 62(8):865–870
52. Srivastava S (2012) Effect of aggregation on thermal conductivity and viscosity of nanofluids. *Appl Nanosci* 2(3):325–331
53. Meister S (2012) grain and particle analysis with line intersection method—File Exchange—MATLAB Central. <http://www.mathworks.com/matlabcentral/fileexchange/35203-grain-and-particle-analysis-with-line-intersection-method>. Accessed 9–26 2014
54. Sathyanarayana S, Hübner C (2013) Thermoplastic nanocomposites with carbon nanotubes. In: Njuguna JJ (ed) *Structural nanocomposites*. Springer, Berlin, pp 19–60
55. Liu R, Ma G, Meng F-T, Su Z-G (2005) Preparation of uniform-sized PLA microcapsules by combining Shirasu Porous Glass membrane emulsification technique and multiple emulsion-solvent evaporation method. *J Control Release* 103(1):31–43
56. Haroosh HJ, Chaudhary DS, Dong Y (2012) Electrospun PLA/PCL fibers with tubular nanoclay: morphological and structural analysis. *J Appl Polym Sci* 124(5):3930–3939
57. Jakus AE, Secor EB, Rutz AL, Jordan SW, Hersam MC, Shah RN (2015) Three-dimensional printing of high-content graphene scaffolds for electronic and biomedical applications. *ACS Nano* 9(4):4636–4648
58. Potnuru A (2013) Low noise, interactive robotic system for psychiatric rehabilitation of children. The University of Texas at Dallas, Richardson
59. Burns A, Tadesse Y The mechanical design of a humanoid robot with flexible skin sensor for use in psychiatric therapy. *SPIE smart structures and materials + nondestructive evaluation and health monitoring*, 2014. International Society for Optics and Photonics, pp 90562H–90511

Publisher's Note Springer Nature remains neutral with regard to jurisdictional claims in published maps and institutional affiliations.